Nat Hazards (2018) 91:267–285
https://doi.org/10.1007/s11069-017-3125-7

ORIGINAL PAPER

Nonlinear dynamics of the sea level time series in the eastern English Channel

F. G. Schmitt[1] · A. Crapoulet[1] · A. Hequette[1] · Y. Huang[2]

Received: 29 January 2017 / Accepted: 14 November 2017 / Published online: 24 November 2017

Abstract Coastal flooding due to surge events represents natural hazards with huge potential consequences for coastal regions. Sea level time series display variations on a large range of timescales, with a deterministic component associated with tidal variations and a stochastic component primarily associated with meteorological forcing, the non-tidal residual. The deterministic component can be evaluated using a model taking into account astronomical forcing and topographic information. The measured sea level is the sum of a slowly varying mean sea level component, the tidal term and the stochastic term. Here, we consider hourly time series recorded in the ports of Boulogne-sur-Mer, Calais, and Dunkirk, in the eastern English Channel. Measured data and modeled data, both provided by the SHOM ("Service hydrographique et océanographique de la marine," hydrographic and oceanographic services of the French Navy), are analyzed using Fourier spectral analysis. The statistics of return times of extreme events are also estimated directly from the time series and compared between modeled and measured data. It is found that return times from tidal or measured time series are quite different for large thresholds and that they also have a very different Fourier power spectrum, the measured data having a power-law regime which is not found in the modeled tidal data. It is also shown, using Hilbert–Huang transform, that non-tidal residual time series are intermittent and possess multifractal scaling properties. Finally, water level non-tidal residual relationship is explored, and it is

✉ F. G. Schmitt
francois.schmitt@cnrs.fr

A. Hequette
arnaud.hequette@univ-littoral.fr

Y. Huang
yongxianghuang@xmu.edu.cn

[1] Univ. Lille, Univ. Littoral Cote d'Opale, UMR 8187, LOG, Laboratoire d'Océanologie et de Géosciences, CNRS, 62 930 Wimereux, France

[2] State key Laboratory of Marine Environmental Science, College of Ocean and Earth Sciences, Xiamen University, Xiamen 361102, China

shown that the larger mean values of the surge (negative and positive parts) are obtained for the medium level of the tidal value.

Keywords Surge · Return times · Sea level · Scaling · Intermittency

1 Introduction

Coastal surges are natural hazards that can lead to considerable casualties and material losses (Baxter 2005; Dube et al. 2009; Melton et al. 2010; Vinet et al. 2013; Shepard et al. 2013). The sea level is a complex signal, with a deterministic part and a stochastic one. The deterministic term is the tidal component, which corresponds to the astronomical influence of the Earth–Moon–Sun system. It is classically modeled using harmonic analysis, as a sum of monochromatic trigonometric terms. The amplitudes of the first and main terms of this harmonic decomposition depend on the shape of the local oceanic basins; they are obtained using numerical methods taking into account the topography and bathymetry (Pugh and Woodworth 2014). The harmonic constants can be numerically estimated in all coastal locations, providing a tidal signal. In France, this is done by the SHOM ("Service hydrographique et océanographique de la marine", hydrographic and oceanographic services of the French Navy): It provides official tidal predictions for all coastal positions of the French littoral. The stochastic component is mainly the surge, which corresponds to the influences of meteorological phenomena. It is the result of generally unknown nonlinear interactions between atmospheric pressure, water and atmospheric temperatures, winds, waves, and turbulence (Pugh 2004; Pugh and Woodworth 2014). For a positive surge, the

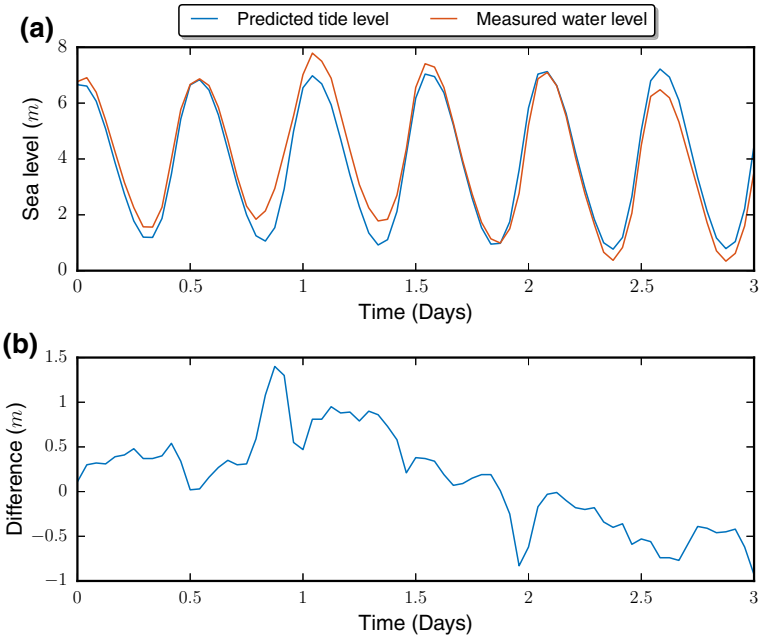

Fig. 1 A typical 3 days portion of the sea level in the eastern English Channel (extract from the Boulogne series). **a** superposition of the theoretical curve and the measured time series. **b** The difference, measured-theory, showing the non-tidal residual component, reaching here values from −1 to +1.5 m

measured sea level is larger than the predicted and calculated one (see Fig. 1, a typical example extracted from the Boulogne series). The most extreme surge levels offshore can reach 7–9 m (Pugh 2004), but are generally much lower along the coasts of France (Ullmann et al. 2007; Bertin et al. 2015).

Here, we consider data recorded in three ports of the North East France. It is a densely populated region with many sandy beaches and coastal dunes. The sea is macro-tidal, with an average tidal range varying from about 4.5–6.2 m along the coast of the region. In this region, storm surges can sometimes exceed 2 m (Chaverot et al. 2008). In such system, a positive surge occurring during a low tide is not dangerous, whereas when the positive surge occurs at or near high-level tide, there can be a dramatic coastal flooding since some parts of the coastal zone, behind protecting coastal dunes, are low-lying and hence quite vulnerable (Hequette 2010; Maspataud et al. 2013). Erosion is also linked to the water level, when waves can reach the coastal dunes, which in normal conditions are not in contact with the sea (Pye and Blott 2008). It has been shown that coastal dunes erosion is strongly dependent on the duration of the positive surge event during a flood (Ruz et al. 2009). The magnitude of the erosion process is strongly linked to the maximum height of the sea level reached during the surge event (Esteves et al. 2012). There are potentially high sea levels for each spring tide, but the largest morphological modifications of the littoral zone, and material damages occur when there is a strong meteorological surge during a high spring tide (Betts et al. 2004; Jones and Davies 2007). This was the case during Xynthia storm that hit the French Atlantic coast in February 2010 (Bertin et al. 2014; Vinet et al. 2013).

A good understanding of the statistical and dynamical properties of the sea level time series is hence needed, in order to better know the frequency and the probability of occurrence of extreme sea levels and to prevent coastal flooding hazards. This is particularly critical for low-lying coastal regions, threatened by marine flooding and changing sea levels (Haigh et al. 2011; Weisse et al. 2012; Maspataud et al. 2013).

Here, we analyze sea level time series from the ports of Boulogne-sur-Mer, Calais, and Dunkirk, both theoretically predicted (tidal model) and measured water levels from tide gauges. The present paper is mainly a methodological contribution, where new methods, borrowed from the fields of turbulence and time series analysis, are applied to water level time series. Below in the first section, the data are presented. Then, the main methods which are used here are presented in the next section. Dynamical and intermittent properties of tidal and measurements time series are presented in the following section: The analyses of power spectra are provided, and then return times of both series are considered. The last section is devoted to the analysis of the surge: the probability density of the surge times series, dynamical properties of the intermittency of surge time series, using Hilbert–Huang transform, and finally tide–surge interactions through the probability of surge data conditioned by the tidal water level.

2 Data sets

The data consist of hourly tide gauge measurements recorded using tidal gauges in the three ports of Boulogne-sur-Mer, Calais, and Dunkirk (Fig. 2). Table 1 provides the dates of beginning and end of the measurements used in the present study. There are missing data, and the last column of the table provides the percentage of present data. Since the predicted series are obtained from a numerical program, they are available for the same

Fig. 2 Map showing the measurements locations in the ports of Boulogne-sur-Mer, Calais, and Dunkirk

Table 1 Information about water level measurement time series

Port	Beginning date	End date	Number of data values	Present data (%)
Boulogne-sur-Mer	9/07/1973	1/1/2012	208,971	62
Calais	2/15/1965	9/10/2011	286,966	70
Dunkirk	6/7/1956	7/20/2010	364,870	77

period, without missing data. For each series, several hundred thousands of data points are available. For some statistical analyses for which time is not a relevant parameter, such as mean, variance, quantiles, probability laws, the fact that there are missing data is not a problem. For dynamical analyses, such as Fourier spectra and return times, analyses are performed for subsets for which the sampling is regular.

As classically considered, the sea level series $X(t)$ can be represented in general as the sum of three terms (Pugh 2004):

$$X(t) = Z_0(t) + T(t) + S(t), \tag{1}$$

where Z_0 is the mean sea level, which increases (or in some locations decreases) slowly with time, T is the tidal part, and S is the non-tidal residual, which corresponds mainly to the surge. A previous study has estimated the mean sea level change in the Dunkirk location as 1.8 mm/year, as an averaged trend given by measurements from 1942 to 2006 (Haigh et al. 2009). At the scales we consider here (from 2 to 5 decades being the largest scale), this makes a signal of amplitude from 3.5 to 9 cm, which is weak compared to surge events. Hence, we do not consider this trend here, and we consider that the theoretical, predicted signal corresponds to $T(t)$, while the measurements are $X(t)$. The difference $X - T = S$ is taken as the non-tidal residual.

3 Methods

In this section, different methods which will be used in the paper are presented: Fourier spectral analysis, return times estimation using the exceedance function, and empirical mode decomposition associated with Hilbert spectral analysis.

3.1 Fourier spectral analysis

Fourier spectral analysis is useful to provide the energy associated with each frequency (Bendat and Piersol 2000). More precisely, $E(f)$ is an energy density where f is the frequency, and $E(f)df$ is the part of the variance of the original signal, whose frequency range belongs to the frequency band df. This is classically estimated using the Fast Fourier Transform (FFT) algorithm, requiring consecutive values, with no missing data. The power spectra are represented here in log–log plot. Deterministic forcing is visible by spikes in the spectrum, noise by horizontal parts in the spectrum, and power-law regimes of the form $E(f) \sim f^{-\beta}$ appear as straight lines of slope β.

3.2 Return times estimated using the exceedance function

Return times are dynamical quantities for a stochastic process, characterizing the recurrence of a given state. For natural phenomena, the concept of return times has a special importance when considering extreme events, which can have huge societal impacts, e. g., storms, earthquakes, floods. Return times correspond to the time between the end of an extreme event and the beginning of the next one. Successive return times can be built from a given time series. If the process considered is stochastic, return times are also stochastic. Of frequent interest is the mean return time associated with a given threshold. The larger the threshold, the larger the mean return time associated with this threshold. It is known for discrete and stationary stochastic processes that the mean return time $\overline{T}$ for a cell A of probability $P(A)$ can be written as (Kac 1947; Nicolis and Nicolis 2007):

$$\overline{T} = \frac{\tau}{P(A)}, \tag{2}$$

where τ is the time step of the process. This result is a theorem, using the hypothesis that the probability of large return time is very small. By considering the events larger than the

threshold, one obtains the complementary cumulative distribution function, or exceedance function:

$$F(x) = \Pr(X > x) \tag{3}$$

where X is the process studied and x the threshold. The mean return is then estimated using $F(x)$. If there are N measurement values, and n_0 occurrences of events larger than the threshold s, then $p = \Pr(X > x) = F(s) = n_0/N$, and the mean return time is written as:

$$\overline{T}(s) = \frac{\tau}{p} = \frac{\tau N}{n_0}. \tag{4}$$

For example, for $N = 10^6$ measurement values, and $n_0 = 10$ occurrences, for hourly data, one has $\overline{T} = 100,000$ h $= 11.4$ years. This approach is useful, since the return times do not need to be directly estimated; one needs only to consider the exceedance function and to estimate from it a mean return time.

3.3 Empirical mode decomposition and Hilbert spectral analysis

The objective of the empirical mode decomposition (EMD) method is to decompose a time series into a sum of modes, each one being narrow banded in frequency. Then, Hilbert spectral analysis (HSA) is applied on each mode time series, in order to extract locally, for each time step, instantaneous amplitude and frequency information. This approach was introduced in the end of the 1990s (Huang et al. 1998) and has since received a large audience, with several thousand citations for the original article. It has been applied on turbulence time series and generalized to study intermittency (Huang et al. 2008, 2011). A recent reference describes in detail the use of EMD and HSA for the study of scaling intermittency (Schmitt and Huang 2016).

The first step is the EMD algorithm, applied on the original time series. The EMD is similar with Fourier or wavelet analysis, but has a main difference, due to the fact that no basis function is assumed a priori: The method is adaptative, meaning that each mode has a different shape, given by the data. However, the method is not mathematically based and relies on an iterative algorithm. We do not provide here all the details on this algorithm and refer to the original paper for this (Huang et al. 1998), or to the recent book detailing the calculation procedure (Schmitt and Huang 2016). The algorithm extracts p modes $C_i, i \in [1, p]$, from high to low frequencies. At the end of the decomposition, the original time series $X(t)$ is the sum of the p modes and a residual $r(t)$:

$$X(t) = \sum_{i=1}^{p} C_i(t) + r(t) \tag{5}$$

The number p is of the order of $\log_2 N$, where N is the number of data points of the original series. This method can be used to filter a series (excluding the first modes corresponding to higher frequencies), or to consider the fluctuations at some given scales (by considering the modes corresponding to these scales) (Flandrin and Gonçalvès 2004). This decomposition is followed by HSA, applied to each mode, in order to locally extract an amplitude and a frequency. A Hilbert transform is applied to each mode:

$$\hat{X}(t) = \frac{1}{\pi} \int \frac{X(u)\mathrm{d}u}{t-u}. \tag{6}$$

This Hilbert transform is used to build a so-called analytical signal as $Z(t) = X(t) + j\hat{X}(t) = A(t)e^{j\theta(t)}$, where $j^2 = -1$, $A(t)$ is the local amplitude and $\theta(t)$ the phase. The derivative of the phase gives the instantaneous frequency $\omega(t) = \theta'(t)/(2\pi)$. This provides a time–frequency–amplitude methodology providing for each time t p values of the amplitude and the phase. A 2D probability density $p(\omega, A)$ is a amplitude–frequency space that can be estimated from the data. This can be used to extract the energy associated with a frequency $h(\omega)$:

$$h(\omega) = \int_0^\infty p(\omega, A)A^2\mathrm{d}A \tag{7}$$

This provides an approach which is similar to the Fourier spectral energy estimation $E(f)$. The comparison between this EMD–HSA method and the Fourier power spectrum has been done first for turbulence data (Huang et al. 2008). Such approach is attractive by the fact that it can be used even when some data are missing, contrary to the classical algorithm for the Fourier transform (the Fast Fourier Transform (FFT)), which requires equally spaced data. A generalization of this approach has been proposed to study the intermittent properties of time series in a new scaling framework (Huang et al. 2008, 2011; Schmitt and Huang 2016). The idea is to consider moments of order $q > 0$ of the amplitude, and not only the second moment. This writes:

$$L_q(\omega) = \int_0^\infty p(\omega, A)A^q\mathrm{d}A \tag{8}$$

In case of scale invariance of the fluctuations, these q order moments of the fluctuations characterize intermittency through a power law as follows:

$$L_q(\omega) \sim \omega^{-\xi(q)}, \tag{9}$$

where $\xi(q)$ is an intermittency exponent, which characterizes the multiscale statistics of the process considered. Larger moments q correspond to larger fluctuations.

It is related to the classical structure functions scaling exponent $\zeta(q)$ (Frisch 1995) by $\xi(q) = \zeta(q) + 1$ (Huang et al. 2008, 2011; Schmitt and Huang 2016). This can also be compared to some classical scaling stochastic models. For example for Brownian motion, $\zeta(q) = q/2$, for fractional Brownian motion, a classical fractional generalization of Brownian motion, $\zeta(q) = qH$, with $0 < H < 1$, where H is the Hurst exponent, which characterizes the scaling of the mean fluctuations. If the moment function is linear, the process is monofractal; the intermittency is larger for multifractal processes, for which the moment function $\zeta(q)$ or $\xi(q)$ is nonlinear and concave. This method has been shown to have less influence from periodic signals superposed to scaling stochastic fluctuations, compared to the classical structure functions analysis (Huang et al. 2011; Schmitt and Huang 2016). It is hence well designed for the analysis of the surge time series, which has less influence from tidal deterministic harmonics than the water level signal itself, but where there are still deterministic peaks remaining.

4 Dynamical and intermittent properties of the tidal times series and of the measurements

4.1 Power spectra

We consider here a first dynamical property of the series $X(t)$ and $T(t)$: their Fourier power spectra. Since the FFT algorithm requires consecutive values, we have taken here for the Fourier spectral analysis, recent subsamples of each series, as long as possible, with no missing values. These are indicated in Table 2: There are about 37,000 points for Boulogne-sur-Mer, 44,000 for Calais, and 32,000 for Dunkirk, which is more than enough to perform a Fourier transform and display the spectral density. The corresponding spectra are shown in Fig. 3a–c. Each figure represents superposed spectra for the tidal signal and the measured signal. For the tidal signal, corresponding to theoretical predictions obtained by modeling, the spectra have been estimated on the same portions of time series as for the measured data.

In each case, the superposition of the two spectra is rather limited: Tidal spectra display the different harmonics used for the numerical calculation; these are mainly discrete spectra, with strong peaks corresponding to frequencies used for the reconstruction of the deterministic tidal signal. Measurement spectra are close to tidal spectra only for some peaks at high frequency. For the rest of the frequencies, and many for low frequencies, both spectra are markedly different; for lower frequencies, the measured time series have spectral energy density 3 to 5 orders of magnitude higher than the spectral energy density of the tidal component. Some scaling regimes can be seen for lower frequencies, with values of β given in Table 2. For the Calais series, the value obtained can be compared to the value of 5/3, which corresponds to the Kolmogorov exponent of fully developed turbulence (Frisch 1995; Pope 2000; Schmitt and Huang 2016). For Boulogne-sur-Mer and Dunkirk, the slopes could be compared to the value of $\beta = 1.27 \pm 0.02$ found for velocity in the atmosphere (Katul and Chu 1998; Calif and Schmitt 2014). However, there is no theoretical explanation to be proposed here to better explain this precise value.

The spectra of sea level measured time series hence possess peaks corresponding to the deterministic tidal forcing, and a scale invariant part corresponding to a stochastic forcing associated with the meteorology. The pressure fluctuations have been analyzed (not shown here): They have a scaling power spectrum with a slope close to $-$ 7/3, as expected in the field of turbulence, showing that the pressure information in itself cannot alone explain such scaling behavior in the water level dynamics. There could be an influence of turbulence, for scales going from hours to months, in this meteorological forcing, corresponding to unknown nonlinear interactions between wind, pressure, and temperature.

Table 2 Information about measurement time series, subsamples without missing values, used for the spectral analysis

Port	Begining mes.	End mes.	Number of data points	Slope β
Boulogne-sur-Mer	4/23/2003	8/7/2007	37,613	1.26 ± 0.18
Calais	6/28/1973	7/3/1978	43,944	1.71 ± 0.16
Dunkirk	1/12/2005	9/3/2008	31,924	1.27 ± 0.09

The power spectral slope as estimated from the low-frequency range is also provided

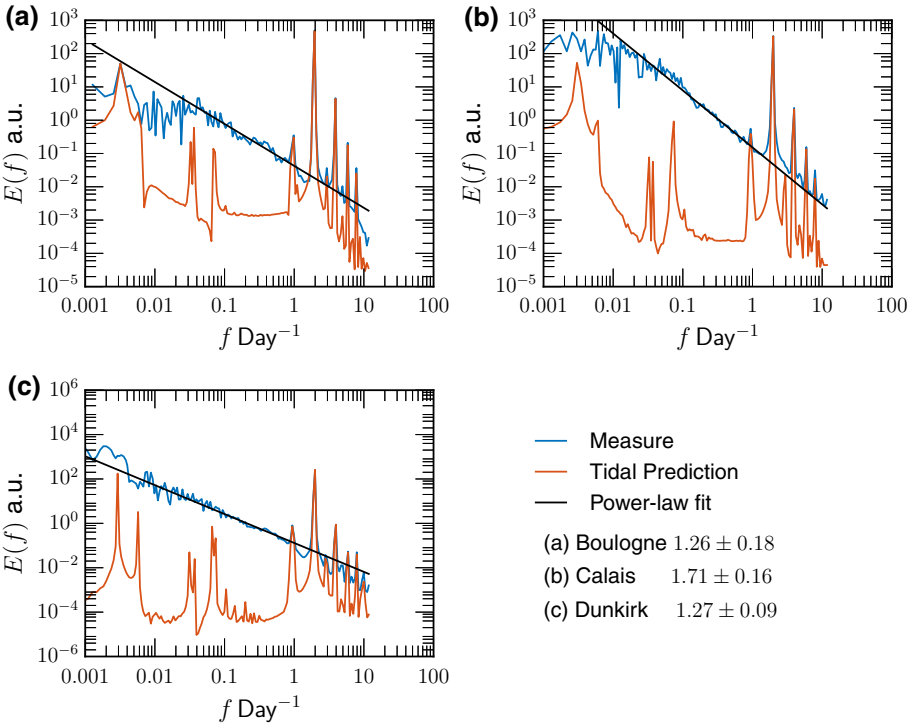

Fig. 3 Spectral analysis of measured and tidal series **a** Boulogne-sur-Mer, **b** Calais, and **c** Dunkirk. Straight lines are also represented, corresponding to power-law fits of the low-frequency part of the measured data. The power-law slopes are given in Table 2

Ideally, for comparison purposes, it would have been better to study the same time periods for the three series, in order to consider the same events. However, the spectral analysis is estimated over periods of several years, which is assumed here to be enough to average out specific meteorological events. It can also be underlined that the effect of longer term variability in sea level data is not captured by such duration time series (Haigh et al. 2011; Mawdsley et al. 2015). However, shorter timescales information is well captured here.

4.2 Return times

Here, another dynamical quantity is considered, the return times for both tidal and measured time series.

Figure 4a represents the exceedance probability estimated for all six time series: tidal model and measurement data in Boulogne, Calais, and Dunkirk. The absolute water level values are different for each port, since the tidal amplitude increases from Dunkirk to Boulogne-sur-Mer. For low threshold values, one can see that, for each series, the probability curves for tidal and measurement data are superimposed. The difference between tidal and measurement data is becoming important and visible only for the larger thresholds, as already found recently (Eelsalu et al. 2014). These curves are transformed

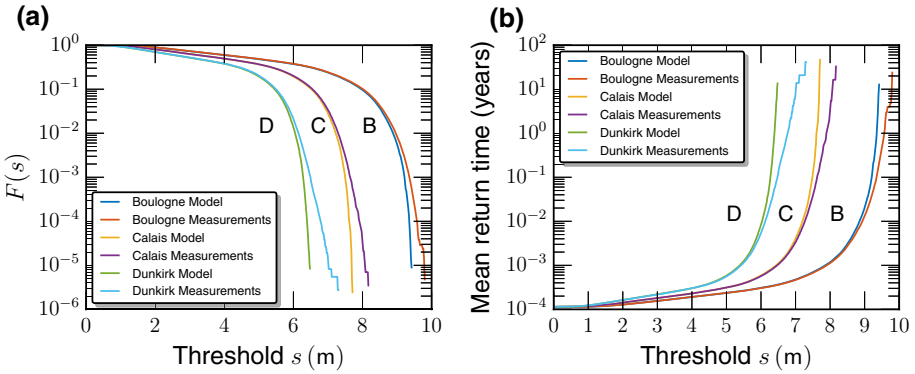

Fig. 4 Left: exceedance probability for the six time series, with each time a comparison between model (tidal data) and measurements (B = Boulogne, C = Calais, D = Dunkirk). Right: transformation of the exceedance probability into a mean return time in years, versus the threshold

into mean return times in Fig. 4b. For large thresholds (larger than 9 m for Boulogne, 7.5 m for Calais, and 6 m for Dunkirk), it is visible that for a given threshold, the mean return time is much larger for the model than for measurements. Inversely, for a given return time, for mean return times larger than 0.02 years = 1 week, the threshold provided by the model and by measurements is different. For example, for a mean return time of 10 years, the threshold is about 40 cm larger for the measurements than for the tidal model.

Finally, let us mention that the extrapolation of such analysis for very large return times is often information requested by local or national authorities. As an example, new dikes are sometimes foreseen, corresponding to a threshold associated with a mean return time of 1000 years. For such estimation, measurements are not long enough, and an extrapolation of the curves must be performed, with an adequate model. Let us emphasize here that the curve obtained for experimental measurements must be used, and not the curve obtained from tidal model data.

The difference for a mean return time of 10 years is 50 cm, and an extrapolation shows that for a mean return time of 100 years, the difference is larger than 1 m, whereas for 1000 years it may reach 4 m. In several aspects, this is a classical problem in coastal engineering and management. It may also be addressed using an ensemble approach (Eelsalu et al. 2014).

4.3 About the pdf of return times

Sometimes engineering consultants or even politics indicate that an event having a mean return time of 100 years has 1/100 probability to happen every year. The general idea is to say that an event having a mean return time of $\overline{T}$ years has a $\tau/\overline{T}$ probability to happen every year (where here $\tau = 1$ year). This is an ambiguous formulation. It is correct to state that the overall probability of such event is $\tau/\overline{T}$, but to indicate that "every year" this is the case, corresponds to assume independence of successive events.

The underlying hypothesis (non stated) is that these events are independent Bernoulli process of parameter $\rho = \tau/\overline{T}$. The probability of not having an event is $1 - \rho = (\overline{T} - \tau)/\overline{T}$, and since each consecutive event is supposed to be independent, the

probability to have k successive "non-events" is $(1-\rho)^k = \left(\frac{\overline{T}-\tau}{\overline{T}}\right)^k$. For $\overline{T}/\tau = 100$ this is 0.99^k. The probability density of return times in this case is an exponential of the form:

$$p(k) = e^{-\lambda k} \tag{10}$$

with $\lambda = \log \frac{\overline{T}}{\overline{T}-\tau}$. For such process, the mean return time has the correct value, since it is $1/\rho = \overline{T}/\tau$. But the pdf of return times or real processes is in general not an exponential. For example, independent extremes follow the Generalized Extreme Value Distribution that is indeed very different from the exponential function: see, e.g., Coles (2004) and Wahl et al. (2017).

This has been verified on a long almost continuous portion, from Dunkirk time series: 112,499 data from September 30, 1997 to July 21, 2010. This portion contains only 0.66% of missing data. The pdf of return times has been estimated for two thresholds: $S = 5$m, for which there is a mean return time of $\overline{T} = 11.3$ h, and 7801 return events, and $S = 6.2$m, for which there is a mean return time of 156.9 h, and 708 different return events. In both cases, a Bernoulli time series of length 5,000,000 data points with parameter $\rho = \tau/\overline{T}$ is generated (here $\tau = 1$ h), and its pdf of return times is compared to the measured ones. Figure 5 shows the exceedance probability $F(x)$ for measured return times, and for a Bernoulli process with the same mean return time. The exponential decrease of the Bernoulli process is clearly visible in each case, whereas the measured exceedance probability has a complex shape, very different from an exponential.

Hence, it is correct to state that the mean return time of an event having a probability of $1/P$ is $\overline{T} = P$, but it is not correct to consider that *every year* its probability of occurring is 1 / P; furthermore, these successive probabilities are not independent.

5 Analysis of the non-tidal residual time series

We analyze here non-tidal residual (NTR) time series, taken as $S(t) = X(t) - T(t)$, the measurements minus the tidal component. Figure 6 shows a portion (from Boulogne-sur-Mer site) of 500 consecutive days of the series $S(t)$, illustrating its stochastic and multiscale

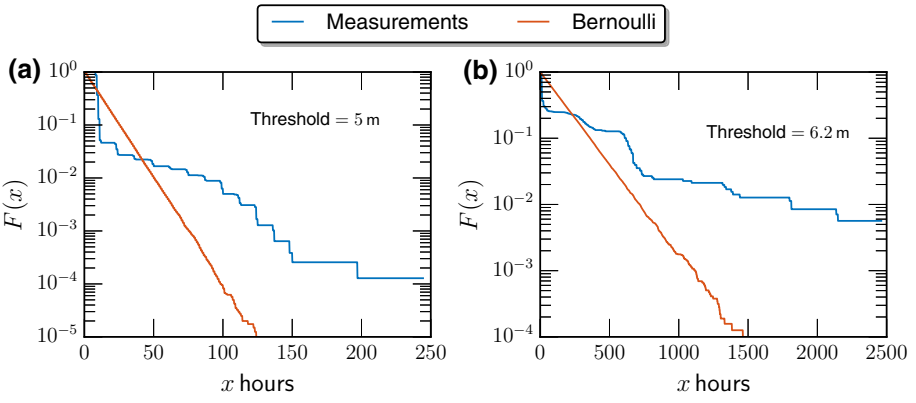

Fig. 5 Exceedance probability $F(x)$ for measured return times, and for a Bernoulli process with the same mean return time. Left: for the threshold $S = 5$ m. Right: the same figure, for the threshold $S = 6.2$ m

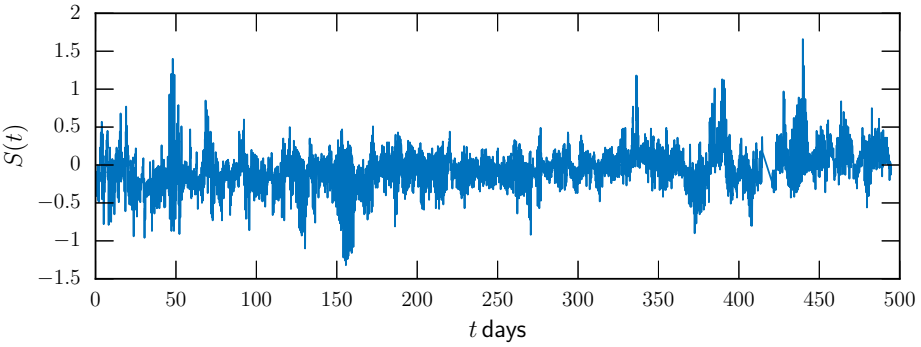

Fig. 6 A portion (from Boulogne-sur-Mer site) of 500 consecutive days of non-tidal residual series $S(t)$. The extract shown here is from November 13, 1975 to March 27, 1977

aspect. We first analyze its statistics, then its dynamical properties, and finally the tide–surge interactions, in the form of the relation between the water level and the non-tidal residual.

5.1 Probability density function of non-tidal residual time series

Table 3 provides the mean, median, standard deviation, minimum, and maximum value of the NTR series for the three ports. The mean and median are very small for each series (of the order of cm); the standard deviation is very similar in each case (of the order of 20 cm). Maxima and minima are very close for Calais and Dunkirk, and for Boulogne-sur-Mer, they are slightly larger. Since there are several hundred thousand data points, the probability density function (PDF) for each series can be estimated with a rather good precision. This is shown in Fig. 7. Both PDFs are superposed, where log of the probability is represented, in order to better visualize the rare events. For positive values, the PDF is very close, and for negative values, the Dunkirk case seems slightly different from the two others. A dotted line is also represented, corresponding to an exponential decrease. The exponential fit is provided by the equation:

$$p(x) = \exp(-K|x|) \tag{11}$$

with the value $K = 6.3$. Some PDF plots of the non-tidal residual can be found in Rabassa and Beck (2015), for the sea levels at various coastal locations in the UK. In this paper, for some plots, an approximate exponential decay can be found, however, with no estimation of the parameter K. An analysis of the variation of the exponent K for both negative and

Table 3 Some statistical values of NTR data for each series

Port	Mean (cm)	Median (cm)	Standard deviation (cm)	Min (cm)	Max (cm)
Boulogne-sur-Mer	2.44	3.0	23.1	− 204	301
Calais	0.5	−1.0	23.6	− 167	223
Dunkirk	1.83	0.0	21.3	− 160	216

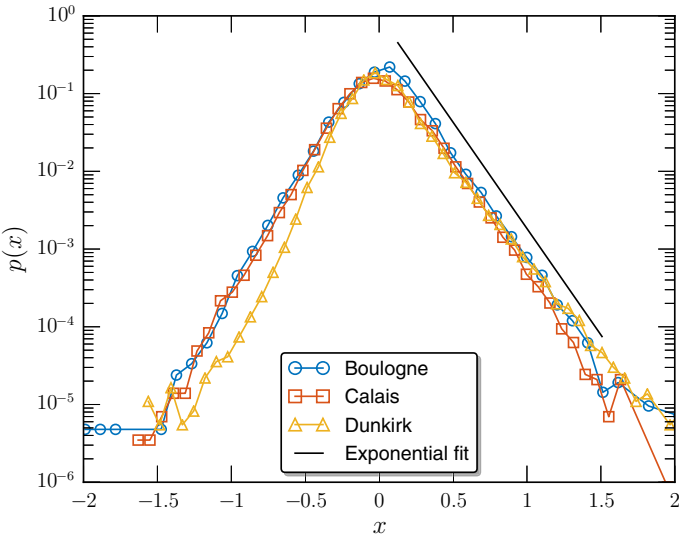

Fig. 7 Probability density function of the non-tidal residual time series, superposed with an exponential fit of equation $p(x) = \exp(-K|x|)$ with $K = 6.3$

positive surges for time series of sea levels numerically reconstructed for the eastern Baltic sea coasts using an ocean model is provided in Soomere et al. (2015).

5.2 Intermittency study of NTR dynamics

We consider here the intermittent properties of the non-tidal residual time series, using the empirical mode decomposition (EMD) methodology, associated with the Hilbert spectral analysis (HSA).

The analysis has been performed on subsamples of the series, for which there are no missing data, as given in Table 2. Hilbert spectral analysis is applied, indicating scaling behavior of the NTR time series, for the range of frequencies $0.03 < \omega < 0.5$ day^{-1} (2 days^{-1} month) (Fig. 8a). Compensated spectra show plateaus for each spectrum, indicating that the scaling is rather well respected (Fig. 8b). The arbitrary order HSA is also applied on the same time series, $L_q(\omega)$ versus ω, and on the same range of frequencies, the exponents $\zeta(q) = \xi(q) - 1$ are extracted with their error bars. The curves $\zeta(q)$ versus the moment q (Fig. 9) are nonlinear in each case, indicating multiscaling behavior of the series. Such property provides a way to generate realistic synthetic time series of surge data. It also characterizes the intermittency of such series, for the scales considered here, from 2 days to 1 month.

5.3 Tide–surge interactions

The relationship between surge and tide has been a topic of interest in many old and recent studies of water level time series (Prandle and Wolf 1978; Horsburgh and Wilson 2007; Bernier and Thompson 2007; Wolf 2009; Idier et al. 2012). The general idea is to consider that surge may have some nonlinear interactions with the tide and that both signals may not be independent. Such result has strong interest in relation to the interpretation and

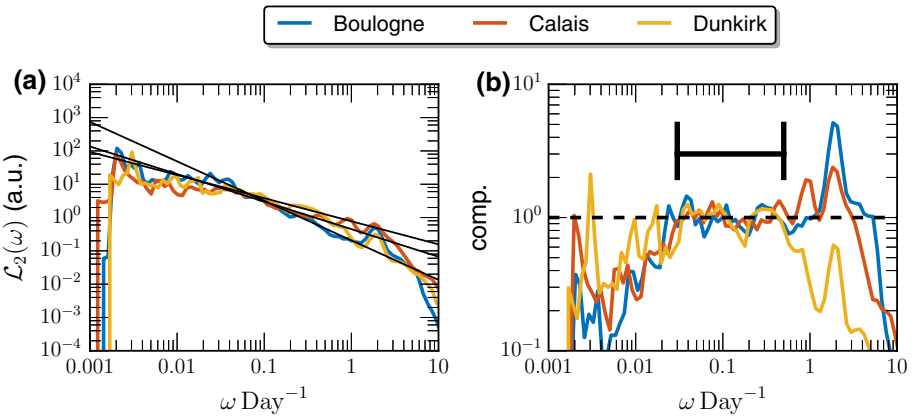

Fig. 8 Energy spectra using HSA analysis, $L_q(\omega)$ versus ω, for all three ports, applied to the subsample of the data, for which there are no missing values, given in Table 2. The scaling range indicated in the figure is $0.03 < \omega < 0.5$ day^{-1} (2 days^{-1} month). The compensated spectra are shown in the figure on the right, the plateaus showing that the scaling is rather well respected

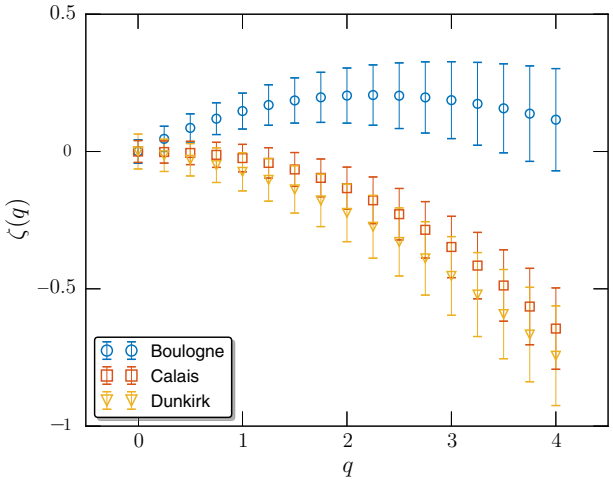

Fig. 9 Scaling exponents $\zeta(q)$ versus the moment q, for all three ports, estimated on the range $0.03 < \omega < 0.5$ day^{-1} (2 days^{-1} month). The error bars are also shown. The nonlinearity indicates multiscaling behavior

prediction of the surge signal. Some of the previous studies have shown that the surge is larger a few hours before the high tide: For example, it has been shown that in the North Sea on the East Coast of England, the peak surges occurrence is 3–5 h before the nearest high water, and sometimes 1–2 h before the nearest high tide (Horsburgh and Wilson 2007).

Here, we do not consider the surge value versus the tidal phase information, since the latter is variable, with many different tidal amplitudes. We prefer to consider, as done in other works, the relation between NTR and height of tide (Haigh et al. 2011; Mawdsley and Haigh 2016). In this framework, we consider something which has not, to our

knowledge, been analyzed before and which is of more direct interest for hazard evaluation: the conditional average of the NTR, with respect to the value predicted by the tidal model). For this, the different tidal level values are partitioned into several classes (25 classes in our analysis, chosen to have enough statistics in each class), and for each class, a conditional mean value of the NTR is estimated. This shows the possible dependency of the NTR value with respect to the tidal level: If there are no dependency, the corresponding curve should be flat. For such analysis, all the available data are considered, as given in Table 1. Figure 10a–c shows the conditional mean NTR for, respectively, Boulogne-sur-Mer, Calais, and Dunkirk. There is clearly a tendency, with large mean NTR values for medium to large values of the tidal level. The same analysis is performed by considering separately positive and negative NTR events. The corresponding curves are shown in the same plots. In each case, the larger mean values of the NTR (negative and positive parts) are obtained for the medium level of the tidal value. The case of Boulogne-sur-Mer is clearer, with mean values of the NTR of 0.2 m for tidal values from 4 to 5 m. The situation in Calais is similar, and in Dunkirk qualitatively less marked. Let us also note that the mean conditional NTR is not the difference between the positive and negative mean conditional curves, since there could be relatively more positive or negative events.

Table 4 presents the total number of positive and negative NTR events, showing that for the Boulogne-sur-Mer case, there are clearly more positive NTR events, whereas for

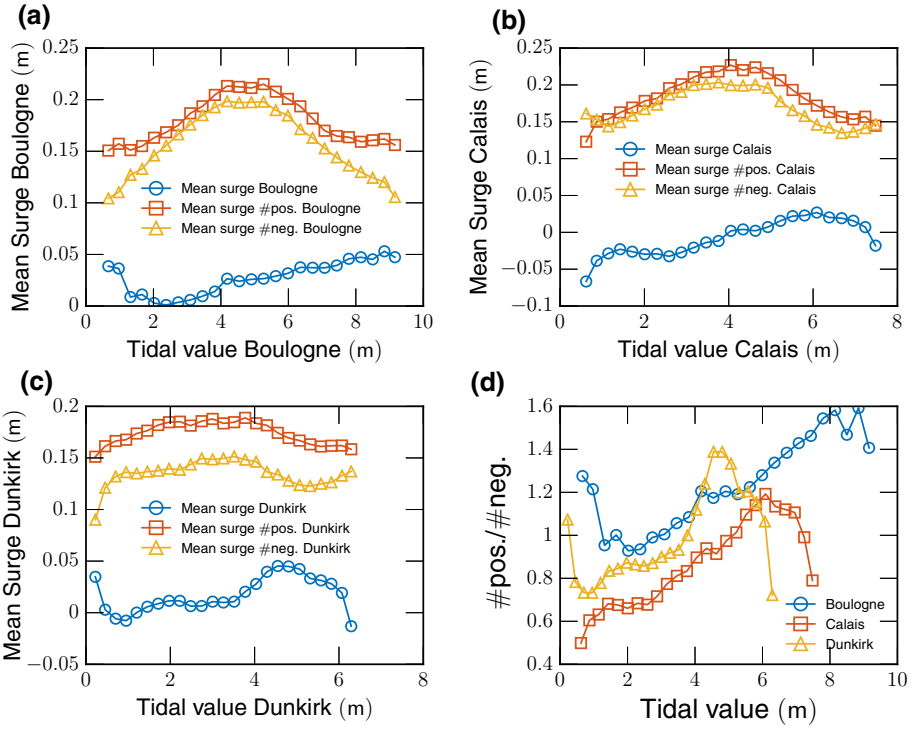

Fig. 10 Conditional average of the NTR, with respect to the absolute tidal level. Top left: Boulogne-sur-Mer, top-right: Calais, bottom-left: Dunkirk. In each case, the mean NTR conditioned on the tidal total water level is displayed, together with the conditional mean of the positive NTR and the conditional mean of the negative NTR. Bottom-right: the ratio of positive to negative number of NTR, for each bin used to consider the conditional mean. Here, the curves for all ports are superposed

Table 4 Information about the number of positive and negative NTR events

Port	Number of data points	Number of positive NTR	Number of negative NTR	Percent pos. NTR (%)
Boulogne-sur-Mer	208,970	113,809	95,161	54.5
Calais	286,966	133,042	153,924	46.4
Dunkirk	364,793	181,322	183,471	49.7

Calais, there are less positive NTR events, and in Dunkirk, there seems to be a relatively even number of positive and negative events. However, these numbers do not necessarily have the same repartition with respect to the tidal level. Indeed, Fig. 10d shows the ratio of positive to negative number of NTR, for each bin used to consider the conditional mean: This shows that there are much more positive NTR events for large tidal values. This is very clear for the Boulogne-sur-Mer case with a rather uniform increase. For the Calais and Dunkirk cases, there is a relative maximum, around 5 m for Calais and 6 m for Dunkirk. This non-uniform number of positive versus negative surge events explains that the difference between conditional positive and negative curves in Fig. 10a–c does not give directly the conditional mean NTR.

6 Discussion and conclusion

Water level time series are complex, multiscale, with a deterministic tidal component and a stochastic part. The deterministic part is a sum of monochromatic trigonometric functions, which amplitudes result from numerical estimations taking into account the geometry of the oceanic basin. The stochastic part is not included in the model and corresponds to meteorological influences. In this paper, we have compared modeled (tidal) and measured time series, in the ports of Boulogne-sur-Mer, Calais, and Dunkirk, in the northern coast of France, in the eastern English Channel, and South of North Sea.

We have first considered the dynamics of both time series, by estimating their Fourier power spectra. For this, we have considered subsamples of the series, for which there are no missing values in the measurements. In each case, power spectra have shown that the model tidal signal is very far from measurements for the low-frequency part, for times larger than 1 day. Only high-frequency peaks are well captured by the model tidal signal. One can also detect a power-law behavior for the measured data, which is visible for two or more decades lower than 1 day^{-1}, with slopes ranging from 1.27 to 1.71. These values could be linked in some way to a turbulence influence, which could be found through pressure, temperature, and wind fields. It is not due to pressure alone, which has a power law close to $-$ 7/3 at these scales. We have also estimated mean return times, using the exceedance probability. We have shown that for large thresholds, mean return times are very different between the tidal model time series and the measurements.

We have also considered the residual, or the surge, which is the difference between the measurements and the tidal signal. We have estimated its probability density function, which is rather close to an exponential distribution, for negative and positive surge events, for all three ports. Its dynamics have been considered for the same subsample, for which there are no missing data, using the empirical mode decomposition and Hilbert spectral

analysis. It was shown to be scaling on a range of scales from 2 days to 1 month, and over this range of scales, the scaling exponents $\zeta(q)$ have been estimated for all three series.

A quantification of the relation between surge and tide has also been realized. Such relation has been explored in other works, mainly by considering the surge events versus the tidal phase. Here, we considered the conditional mean of surge, of positive surges and of negative surges, with respect to the tidal absolute level. We also explored the number of positive or negative surges, with respect to the tidal level.

These approaches are new methodologies. They have been tested here on three times series from ports in Northern France. A perspective of this work is to extend the analysis to other water level series in the English Channel and the North Sea. These methodologies provide a quantitative expression of the dependency between surge and tide, which can be used for predictions of future surges. Such perspectives of the current work can be explored in two directions. On the one hand, synthetic water level series can be generated, with the generation of stochastic NTR variables having correct statistics and dynamics, which are added to the tidal level prediction model. On the other hand, the shape of the mean return time estimated from such series can be compared to measurements and extended in order to provide information on the thresholds associated with much longer mean return times.

We have not considered the slow elevation of the mean sea level. Several studies have shown that the mean sea level elevation is approximately 1.8 mm per year in Dunkirk (Hequette 2010; Haigh et al. 2011). This is a rather weak signal, compared to the high values reached by the surge data (1 or 2 m). A few millimeter trend will not change the exceedance probability at a scale of few years. However, if sea level continues to rise at similar rates or higher over several decades, the mean return times of extreme water levels will necessarily decrease (see discussions in, e.g., Haigh et al. 2011; Mudersbach et al. 2013; Soomere and Pindsoo 2016). In such case, this can be easily incorporated in the present analysis and modeling.

Finally, let us note that the topic of return times is a complex question, especially for time series presenting a strong variability at many different scales. There is a rather strong potential societal impact, via the risk evaluation and political decisions that need to be taken in answer of hazard assessments. Researchers must be careful enough to use well-defined concepts and methods. For a stochastic process, return times are also stochastic. If the last big event was in 1950 and if the estimated mean return time of such event is 70 years, it does not mean that it has a large probability to occur in 2020. Successive return times for a same threshold may have very different magnitudes, and there may be large fluctuations around the mean value. The different results which have been obtained here may provide a methodology to assess the possible universal properties of the surge, and also approaches for stochastic modeling of this complex series for hazard assessment in response to societal needs.

Acknowledgements We thank Denis Marin for the making of Fig. 2. Observations from the tide gauge of Dunkirk are the property of SHOM and the Grand Port Maritime de Dunkirk; observations from the Calais tide gauge are the property of SHOM, the Region "Hauts de France" and of the port of Calais; observations from the Boulogne-sur-Mer tide gauge are the property of SHOM, the Region "Hauts de France-Nord-Pas de Calais Picardie" and of the port of Boulogne-sur-Mer. These datasets are available on the Web site of the reference network of tide gauge observations (https://refmar.shom.fr). The reviewers are thanked for their comments and recommendations that helped improve the manuscript. Y.X is partially sponsored by the National Natural Science Foundation of China (under Grant Nos. 11332006 and 11732010) and by the Fundamental Research Funds for the Central Universities (Grant No. 20720150075). Y.X. and F.G.S. are partially funded by the Sino-French (NSFC-CNRS) joint research project LATUMAR (No. 11611130099, NSFC China, and PRC 2016-2018).

References

Baxter PJ (2005) The east coast Big Flood, 31 January–1 February 1953: a summary of the human disaster. Philos Trans R Soc A 363:1293–1312

Bendat JS, Piersol AG (2000) Random data, analysis and measurement procedures, 3rd edn. Wiley, Hoboken

Bernier NB, Thompson KR (2007) Tide–surge interaction off the east coast of Canada and northeastern United States. J Geophys Res 112:C06008

Bertin X, Li K, Roland A, Zhang YJ, Breilh J-F, Chaumillon E (2014) A modeling-based analysis of the flooding associated with Xynthia, central Bay of Biscay. Coast Eng 94:80–89

Bertin X, Li K, Roland A, Bidlot J-R (2015) The contribution of short-waves in storm surges: two case studies in the Bay of Biscay. Cont Shelf Res 96:1–15

Betts NL, Orford JD, White D, Graham CJ (2004) Storminess and surges in the South-Western approaches of the eastern North Atlantic: the synoptic climatology of recent extreme coastal storms. Mar Geol 210:227–246

Calif R, Schmitt FG (2014) Multiscaling and joint multiscaling description of the atmospheric wind speed and the aggregate power output from a wind farm. Nonlinear Process Geophys 21:379–392

Chaverot S, Hequette A, Cohen O (2008) Changes in storminess and shoreline evolution along the northern coast of France during the second half of the 20th century. Z Geomorphol suppl 52:1–20

Coles S (2004) An introduction to statistical modeling of extreme values. Springer, Berlin

Dube SK, Indu Jain, Rao AD, Murty TS (2009) Storm surge modelling for the Bay of Bengal and Arabian Sea. Nat Hazards 51:3–27

Eelsalu M, Soomere T, Pindsoo K, Lagemaa P (2014) Ensemble approach for projections of return periods of extreme water levels in Estonian waters. Cont Shelf Res 91:201–210

Esteves LS, Brown JM, Williams JJ, Lymbery G (2012) Quantifying thresholds for significant dune erosion along the Sefton Coast, Northwest England. Geomorphology 143–144:52–61

Flandrin P, Gonçalvès P (2004) Empirical mode decompositions as data-driven wavelet-like expansions. Int J Wavelets Multiresolut Inf Process 2(4):477–496

Frisch U (1995) Turbulence: the legacy of AN Kolmogorov. Cambridge University Press, Cambridge

Haigh I, Nicholls RJ, Wells NC (2009) Mean sea level trends around the English Channel over the 20th century and their wider context. Cont Shelf Res 29:2083–2098

Haigh I, Nicholls R, Wells N (2011) Rising sea levels in the English Channel 1900 to 2100. Marit Eng 164(MA2):81–92

Hequette A (2010) Les risques naturels littoraux dans le Nord-Pas-de-Calais, France, VertigO, hors ser. 8

Horsburgh KJ, Wilson C (2007) Tide-surge interaction and its role in the distribution of surge residuals in the North Sea. J Geophys Res 112:C08003

Huang NE, Shen Z, Long SR, Wu MC, Shih HH, Zheng Q, Yen N, Tung CC, Liu HH (1998) The empirical mode decomposition and the Hilbert spectrum for nonlinear and non-stationary time series analysis. Proc R Soc London 454(1971):903–995

Huang Y, Schmitt FG, Lu Z, Liu Y (2008) An amplitude-frequency study of turbulent scaling intermittency using Hilbert spectral analysis. EPL 84:40010

Huang Y, Schmitt FG, Hermand J-P, Gagne Y, Lu ZM, Liu YL (2011) Arbitrary order Hilbert spectral analysis for time series possessing scaling statistics: a comparison study with detrended fluctuation analysis and wavelet leaders. Phys Rev E 84:016208

Idier D, Dumas F, Muller H (2012) Tide-surge interaction in the English Channel. Nat Hazards Earth Syst Sci 12:3709–3718

Jones JE, Davies AM (2007) Influence of non-linear effects upon surge elevations along the west coast of Britain. Ocean Dyn 57:401–416

Kac M (1947) On the notion of reccurence in discrete stochastic processes. Bull Am Math Soc 53:1002–1010

Katul G, Chu CR (1998) A theoretical and experimental investigation of energy-containing scales in the dynamics sublayer of boundary-layer flows. Bound Layer Meteorol 86:279–312

Maspataud A, Ruz M-H, Vanhée S (2013) Potential impacts of extreme storm surges on a low-lying densely populated coastline: the case of Dunkirk area, Northern France. Nat Hazards 66:1327–1343

Mawdsley RJ, Haigh ID (2016) Spatial and temporal variability and long-term trends in skew surges globally. Front Mar Sci 3:29

Mawdsley RJ, Haigh ID, Wells NC (2015) Global secular changes in different tidal high waters, low water and range levels. Earth Future 3:66–81

Melton G, Gall M, Mitchell JT, Cutter SL (2010) Hurricane Katrina storm surge delineation: implications for future storm surge forecasts and warnings. Nat Hazards 54:519–536

Mudersbach C, Wahl T, Haigh ID, Jensen J (2013) Trends in high sea levels of German North Sea gauges compared to regional mean sea level changes. Cont Shelf Res 65:111–120
Nicolis G, Nicolis C (2007) Foundations of complex systems; nonlinear dynamics, statistical physics, information and prediction. World Scientific, London
Pope SB (2000) Turbulent flows. Cambridge University Press, Cambridge
Prandle D, Wolf J (1978) The interactions of surge and tide in the North Sea and River Thames. Geophys J R Astron Soc 55:203–216
Pugh D (2004) Changing sea level. Cambridge University Press, Cambridge, p 265
Pugh D, Woodworth P (2014) Sea level science. Cambridge University Press, Cambridge, p 407
Pye K, Blott SJ (2008) Decadal-scale variation in dune erosion and accretion rates: an investigation of the significance of changing storm tide frequency and magnitude on the Sefton coast. Geomorphology 102:652–666
Rabassa P, Beck C (2015) Superstatistical analysis of sea-level fluctuations. Physica A 417:18–28
Ruz M-H, Hequette A, Maspataud A (2009) Identifying forcing conditions responsible for foredune erosion on the northern coast of France. J Coastal Res SI 56:356–360
Schmitt FG, Huang Y (2016) Stochastic analysis of scaling time series: from turbulence theory to applications. Cambridge University Press, Cambridge
Shepard CC, Agostini VN, Gilmer B, Allen T, Stone J, Brooks W, Beck MW (2013) Assessing risk associated with sea-level rise and storm surge-redux. Nat Hazards 65:375–376
Soomere T, Pindsoo K (2016) Spatial variability in the trends in extreme storm surges and weekly-scale high water levels in the eastern Baltic Sea. Cont Shelf Res 115:53–64
Soomere T, Eelsalu M, Kurkin A, Rybin A (2015) Separation of the Baltic Sea water level into daily and multi-weekly components. Cont Shelf Res 103:23–32
Ullmann A, Pirazzoli PA, Tomasin A (2007) Sea surges in Camargue: Trends over the 20th century. Cont Shelf Res 27:922–934
Vinet F, Lumbroso D, Defossez S, Boissier L (2013) A comparative analysis of the loss of life during two recent floods in France: the sea surge caused by the storm Xynthia and the flash flood in Var. Nat Hazards 61:1179–1201
Wahl T, Haigh ID, Nicholls RJ, Arns A, Dangedorf S, Hinkel J, Slangen ABA (2017) Understanding extreme sea levels for broad-scale coastal impact and adaptation analysis. Nat Commun 8:16075
Weisse R, von Storch H, Niemeyer HD, Knaack H (2012) Changing North Sea storm surge climate: an increasing hazard? Ocean Coast Manag 68:58–68
Wolf J (2009) Coastal flooding: impacts of coupled wave-surge-tide models. Nat Hazard 49:241–260